EUROPEAN ORGANIZATION FOR NUCLEAR RESEARCH

Measurement of visible cross sections in proton-lead collisions at $\sqrt{s_{NN}}$ = 5.02 TeV in van der Meer scans with the ALICE detector

The ALICE Collaboration[*]

Abstract

In 2013, the Large Hadron Collider provided proton-lead and lead-proton collisions at the center-of-mass energy per nucleon pair $\sqrt{s_{NN}}$ = 5.02 TeV. Van der Meer scans were performed for both configurations of colliding beams, and the cross section was measured for two reference processes, based on particle detection by the T0 and V0 detectors, with pseudo-rapidity coverage $4.6 < \eta < 4.9$, $-3.3 < \eta < -3.0$ and $2.8 < \eta < 5.1$, $-3.7 < \eta < -1.7$, respectively. Given the asymmetric detector acceptance, the cross section was measured separately for the two configurations. The measured visible cross sections are used to calculate the integrated luminosity of the proton-lead and lead-proton data samples, and to indirectly measure the cross section for a third, configuration-independent, reference process, based on neutron detection by the Zero Degree Calorimeters.

---

[*]See Appendix A for the list of collaboration members

1   Introduction

Luminosity determination in ALICE (A Large Ion Collider Experiment) [1] at the LHC is based on visible cross sections measured in van der Meer (vdM) scans [2, 3]. The visible cross section σ_{vis} seen by a given detector (or set of detectors) with a given trigger condition is a fraction of the total inelastic interaction cross section σ_{inel}: $\sigma_{\mathrm{vis}} = \varepsilon \sigma_{\mathrm{inel}}$, where ε is the fraction of inelastic events which satisfy the trigger condition. In the following, an inelastic event satisfying a given trigger condition will be referred to as a reference process. Once the reference-process cross section (σ_{vis}) is measured, the collider luminosity can be determined as the reference-process rate divided by σ_{vis}. This procedure does not require knowledge of ε.

In vdM scans the two beams are moved across each other in the transverse directions x and y. Measurement of the rate R of the reference process as a function of the beam separation Δx, Δy allows one to determine the luminosity L for head-on collisions of a pair of bunches with particle intensities N_1 and N_2 as

$$L = N_1 N_2 f_{\mathrm{rev}}/(h_x h_y), \tag{1}$$

where f_{rev} is the accelerator revolution frequency and h_x and h_y are the effective beam widths in the two transverse directions. The effective beam widths are measured as the area below the $R(\Delta x, 0)$ and $R(0, \Delta y)$ curve (scan area), respectively, each divided by the head-on rate $R(0,0)$. Under the assumption that the beam profiles are Gaussian, the effective width is obtained as the Gaussian standard deviation parameter (from a fit) multiplied by $\sqrt{2\pi}$. However, the Gaussian assumption is not necessary for the validity of the method. As will be shown in section 3, other functional forms can be used, as well as numerical integration of the curve. The cross section σ_{vis} for the chosen reference process is then

$$\sigma_{\mathrm{vis}} = R(0,0)/L. \tag{2}$$

In 2013, the Large Hadron Collider provided proton-lead and lead-proton collisions at the center-of-mass energy per nucleon pair $\sqrt{s_{\mathrm{NN}}} = 5.02$ TeV. Van der Meer scans were performed for both configurations of colliding beams, and the cross section was measured for two reference processes. In section 2, the detectors used for the measurements are briefly described, along with the relevant machine parameters and the adopted scan procedure. In section 3, the analysis procedure is described. In section 4, the obtained results and uncertainties are presented and discussed. In section 5, the application of the vdM scan results to the measurement of the integrated luminosity is briefly discussed. In section 6, the vdM scan results are used to indirectly determine the cross section for a third reference process, based on neutron detection by the ALICE Zero Degree Calorimeters.

2   Experimental setup

At the ALICE experiment, two vdM-scan sessions were carried out during the 2013 proton-lead data-taking campaign at the LHC. The proton beam was travelling clockwise in the first session and counter-clockwise in the second session. In the following, these configurations will be referred to as p–Pb and Pb–p, respectively.

In each session, the cross section was measured for two reference processes: one is based on the V0 detector, the other on the T0 detector. A detailed description of these detectors is given in [1], and their performance is discussed in [4], [5] and [6]. The V0 detector consists of two hodoscopes, with 32 scintillator tiles each, located on opposite sides of the ALICE Interaction Point (IP2), at a distance of 340 cm (V0-A) and 90 cm (V0-C) along the beam axis, covering the pseudo-rapidity (η) ranges $2.8 < \eta < 5.1$ and $-3.7 < \eta < -1.7$, respectively. In the p–Pb configuration the proton beam is travelling in the direction from V0-A to V0-C. The T0 detector consists of two arrays of 12 Cherenkov counters each, located on opposite sides of IP2, at a distance of 370 cm (T0-A) and 70 cm (T0-C) along the beam

axis, covering the pseudo-rapidity ranges $4.6 < \eta < 4.9$ and $-3.3 < \eta < -3.0$, respectively. In the p–Pb configuration the proton beam is travelling in the direction from T0-A to T0-C.

The V0-based trigger condition, chosen as the reference process, requires at least one hit in each detector hodoscope, i.e. on both sides of IP2. As discussed in [7], the efficiency of such a selection is larger than 99% for non single-diffractive p–Pb collisions. A similar trigger condition defines the T0-based reference process, with the additional condition that the longitudinal coordinate of the interaction vertex, evaluated by the trigger electronics via the difference of arrival times in the two arrays (measured with a resolution of 20 ps), lies in the range $|z| < 30$ cm (where $z = 0$ is the nominal IP2 position). This online cut aims to reject the background from beam-gas and beam-satellite interactions. The cut value of 30 cm is much larger than the r.m.s. longitudinal size of the interaction region ($\simeq 6$ cm), making signal loss induced by the cut negligible ($<10^{-5}$). Since the two LHC beams have the same magnetic rigidity and different projectile mass, the energy per nucleon of lead ions (1.58 TeV) differs from that of protons (4 TeV). Hence, the p–Pb (Pb–p) collision center-of-mass frame is shifted by 0.47 (-0.47) units of rapidity with respect to the ALICE frame. Due to this shift and the asymmetric setup of both detectors, there is no reason to expect identical cross sections for the p–Pb and Pb–p configurations. Therefore, the results obtained in the two scan sessions are not combined.

In the p–Pb (Pb–p) scan session the proton beam consisted of 272 bunches, while the Pb beam consisted of 338 (314) bunches. In the p–Pb (Pb–p) scan session 264 (244) bunch pairs per LHC orbit were colliding at IP2. For both beams and sessions, the minimum spacing between two consecutive bunches was 200 ns. The reference-process rates were recorded (and the cross section measured) separately for each colliding bunch pair. For each session, two independent measurements per bunch pair were performed by repeating the (horizontal and vertical) scan pair twice: from negative to positive separation and then in the opposite direction. The maximum beam separation during the scan was about 0.15 mm, corresponding to about six times the RMS of the transverse beam profile. In both sessions, the β^* value[1] in IP2 was 0.8 m. The current in the ALICE solenoid (dipole) was 30 kA (6 kA), corresponding to a field strength of 0.5 T (0.7 T). In both sessions, the proton and lead bunch intensities were on the order of 10^{10} p/bunch and 10^8 Pb/bunch, as shown in figure 1. While the proton bunch intensity is reasonably constant across bunches, large variations are seen for the lead bunches. The structure of such variations as a function of the bunch position can be explained by different sensitivities to losses in the injection chain [8].
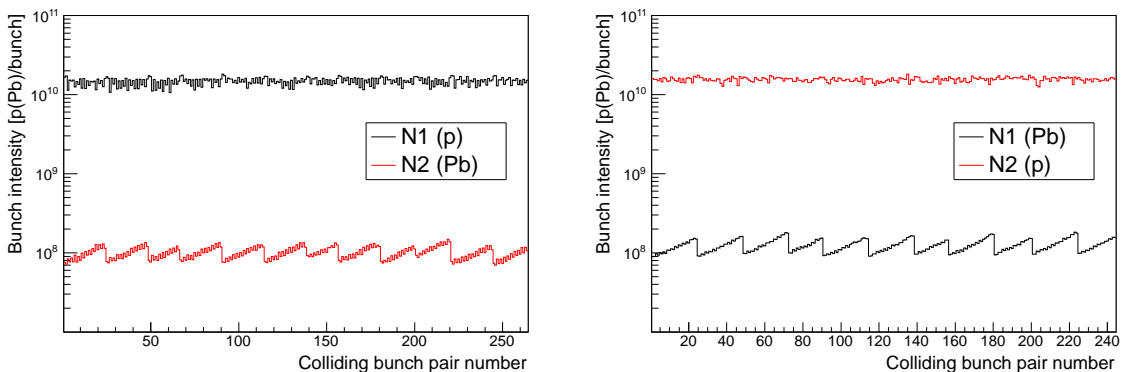

Fig. 1: (Colour online) Bunch intensities N_1 and N_2 for all colliding bunches, for an arbitrary timestamp during the p–Pb (left) and Pb–p (right) scan sessions.

The bunch-intensity measurement is provided for both scan sessions by the LHC instrumentation [9]:

---

[1]The $\beta(z)$ function describes the single-particle motion and determines the variation of the beam envelope as a function of the coordinate along the beam orbit (z). The notation β^* denotes the value of the β function at the interaction point.

a DC current transformer (DCCT), measuring the total beam intensity, and a fast beam current transformer (fBCT), measuring the relative bunch populations. The measured beam intensity is corrected by the fraction of ghost and satellite charge[2]. The measurement of ghost charge is provided by the LHCb collaboration, via the rate of beam-gas collisions occurring in nominally empty bunch slots, as described in [11]. The obtained ghost-charge correction factor to the bunch-intensity product N_1N_2 is 0.991±0.001 (0.986±0.002) for the p–Pb (Pb–p) session. The bunch intensity is further corrected by the fraction of satellite charge measured by the LHC Longitudinal Density Monitor (LDM), which measures synchrotron radiation photons emitted by the beams [12]. The obtained satellite-charge correction factor to the bunch-intensity product N_1N_2 is 0.998±0.004 (0.996±0.001) for the p–Pb (Pb–p) session. This correction is implemented by multiplying the N_1N_2 product by both the ghost- and satellite-charge factors.
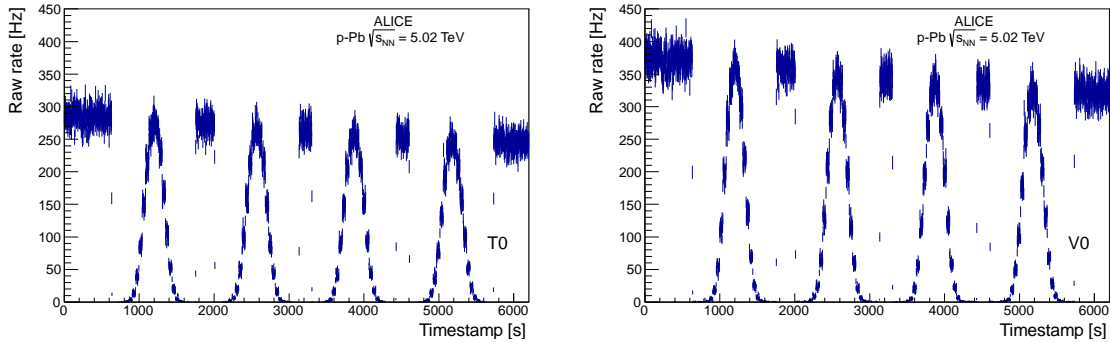

Fig. 2: (Colour online) Raw rate of the T0 (left) and V0 (right) process for a typical colliding bunch pair, as a function of time, during the p–Pb scan session. In each plot, the first (second) bell-shaped structure corresponds to the beam separation in the horizontal (vertical) direction being varied from negative to positive values. The third (fourth) bell-shaped structure corresponds to the beam separation in the horizontal (vertical) direction being varied from positive to negative values.

3   Data analysis

An example of the measured raw rate for one typical pair of colliding bunches during the p–Pb scan is shown in figure 2 for both the T0- and the V0-based processes.

Three corrections are applied to the measured raw rate for each of the two reference processes.

First, the contamination from beam–satellite and beam–gas interactions in the V0 rate is removed using the detector timing capabilities. The background is identified via the sum and difference of arrival times in the two V0 arrays from offline analysis of the data collected during the scan. The arrival times are obtained by averaging over the signal times of all hits of each array. The background contamination is measured as the fraction of events in which the sum and difference of times lie outside of a window of ±4 ns around the values expected for beam-beam collisions (figure 3). The measurement is performed for each separation value and the corresponding raw rate is corrected by the obtained fraction. The background contamination in the V0-triggered sample is about 0.5-1% at zero separation and about 20-40% at a separation corresponding to five times the beam RMS. This procedure has negligible effect ($< 0.1\%$) when applied to the T0 rates, due to the vertex cut in the T0 trigger logic described in section 2.

---

[2]The radio-frequency (RF) configuration of the LHC is such that the accelerator orbit is divided in 3564 slots of 25 ns each. Each slot is further divided in ten buckets of 2.5 ns each. In nominally filled slots, the particle bunch sits in the central bucket of the slot. Following the convention established in [10], the charge circulating outside of the nominally filled slots is referred to as ghost charge; the charge circulating within a nominally filled slot but not sitting in the central bucket is referred to as satellite charge.
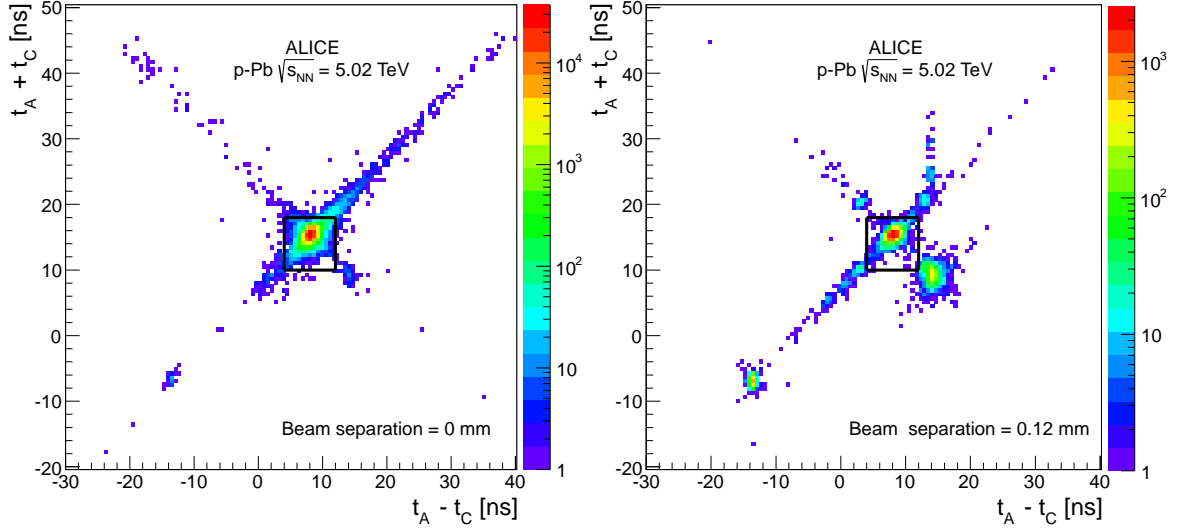
Fig. 3: (Colour online) Correlation between the sum and difference of arrival times (relative to the bunch crossing) on the two V0 arrays. The left plot was obtained at zero beam separation; the right plot was obtained at a beam separation of 0.12 mm, roughly corresponding to five times the RMS of the beam profile. Events lying inside the area within the continuous lines are flagged as beam-beam interactions.

In order to study a possible contamination of the trigger rate from the intrinsic noise counts of the detectors, the rate of both trigger signals in absence of beam was measured and found to be zero. The rate in empty bunch slots with beam circulating was also measured and found to be zero for T0. For V0, a non-zero rate is measured up to the fourth empty bunch slot after a filled slot. Since the minimum spacing between filled slots is eight slots, such an after-pulsing effect does not affect the measurement of the rate in colliding slots.

Second, the probability of multiple interactions in the same bunch crossing (pileup) is taken into account according to Poisson statistics. The trigger rate R is smaller than the rate of visible interactions by a factor $[1 - \exp(-\mu_{vis})]/\mu_{vis}$, where $\mu_{vis} = -\ln(1 - R/f_{rev})$ is the average number of visible interactions occurring in one bunch crossing. The pileup-corrected rate for bunch crossing i, $R_{PU,i}$, is thus given by

$$R_{PU,i} = -f_{rev} \ln(1 - R_{BB,i}/f_{rev}) \tag{3}$$

where $R_{BB,i}$ is the background-corrected rate. In both scan sessions, the maximum value of μ_{vis} during the scan for the V0 (T0) reference process is about 0.05 (0.03), leading to a maximum correction of about 2.5% (1.5%).

The third correction takes into account that the luminosity decreases with time (as can be seen in figure 2) due to the beam-intensity decay and to the growth of emittances. In order to correct for this effect, the evolution of the head-on luminosity in time is parameterised via a fit to the rates at zero separation measured before, after and in-between scans. The decay rate is satisfactorily described by an exponential function. Figure 4 shows an example of such a fit. The obtained fit parameters are used to normalize all rates of a given scan pair to an arbitrary reference time, chosen to lie between the horizontal and vertical scans.

An example of the obtained correction factors as a function of the beam separation is shown in figure 5.

The corrected rates obtained with the above-described procedure are used to compute the effective beam widths h_x and h_y. This is done with both a fit and a numerical method. For the fit method, it was found that a Gaussian (or double-Gaussian) function does not describe satisfactorily the measured shapes, while
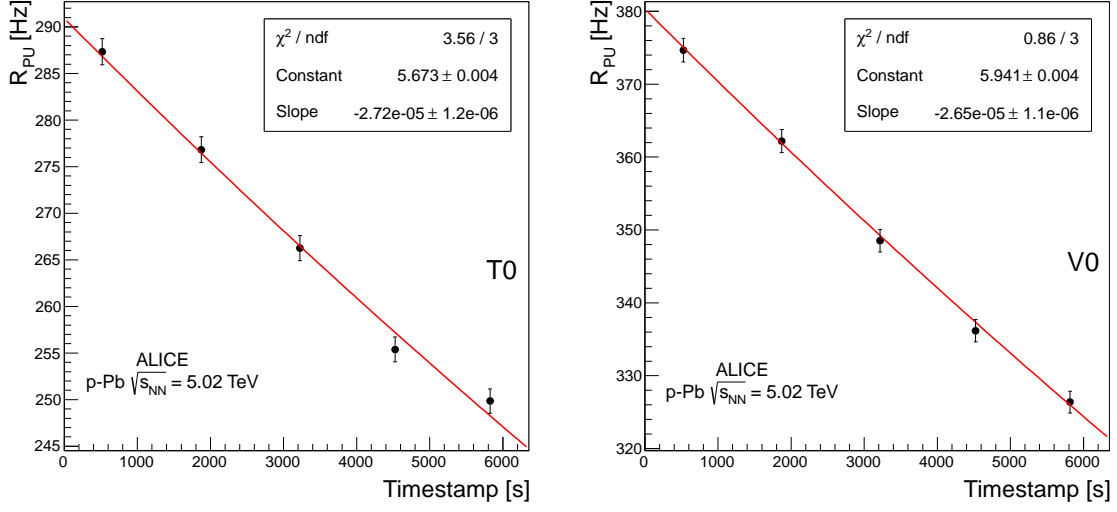
Fig. 4: (Colour online) Background- and pileup-corrected head-on rates of the T0 (left) and V0 (right) reference process as a function of time for one interacting bunch crossing in the p–Pb scan session. The solid red curve is an exponential fit to the data points.
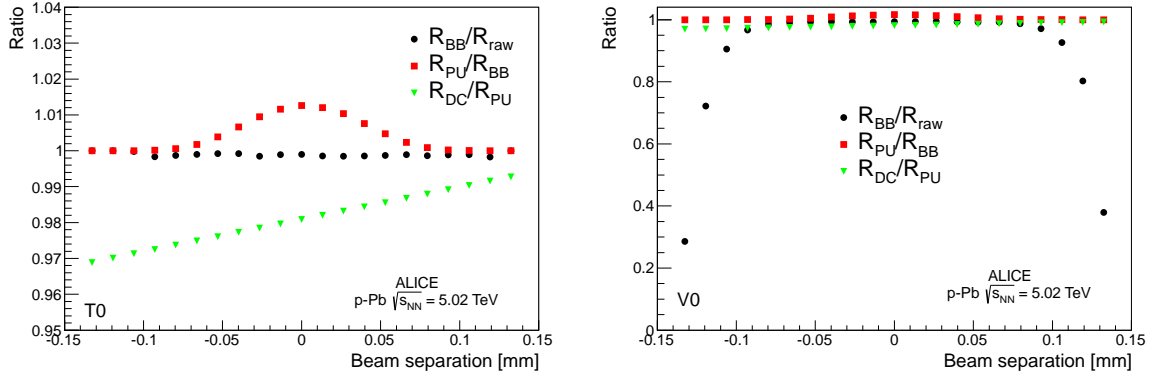

Fig. 5: (Colour online) Background (R_{BB}/R_{raw}), pileup (R_{PU}/R_{BB}) and luminosity decay (R_{DC}/R_{PU}) correction factors to the T0 (left) and V0 (right) rates as a function of the beam separation for one typical pair of colliding bunches during the first p–Pb vertical scan. Due to the different size of the background correction factor for T0 and V0, the two figures have different vertical scales.

reasonable values of χ^2 per degree of freedom (typically <2) are obtained by using a modified Gaussian function

$$R(\Delta x, 0) = R(0,0) \exp\left[-(\Delta x - \mu)^2/2\sigma^2\right] \left(1 + p_2\Delta x^2 + p_4\Delta x^4 + p_6\Delta x^6\right) \qquad (4)$$

and a similar one for $R(0, \Delta y)$. An example of the quality of the fit is shown in figure 6. In the fit approach, the scan area and the head-on rate $R(0,0)$ are obtained from the fit parameters. In the numerical method, the scan area is obtained as the sum of all rates multiplied by the step size, and $R(0,0)$ is the measured rate at zero separation. The effective beam widths and head-on rates obtained with the two methods agree within 0.5%. Since the effective beam widths are independent of the process used to measure them, a consistency check is performed by computing the ratio of the widths obtained with T0 and V0, for each colliding bunch. The results are shown in figure 7 for the p–Pb scan. Although the average value of the ratios is compatible with unity, fluctuations beyond statistical uncertainties are observed, which are taken
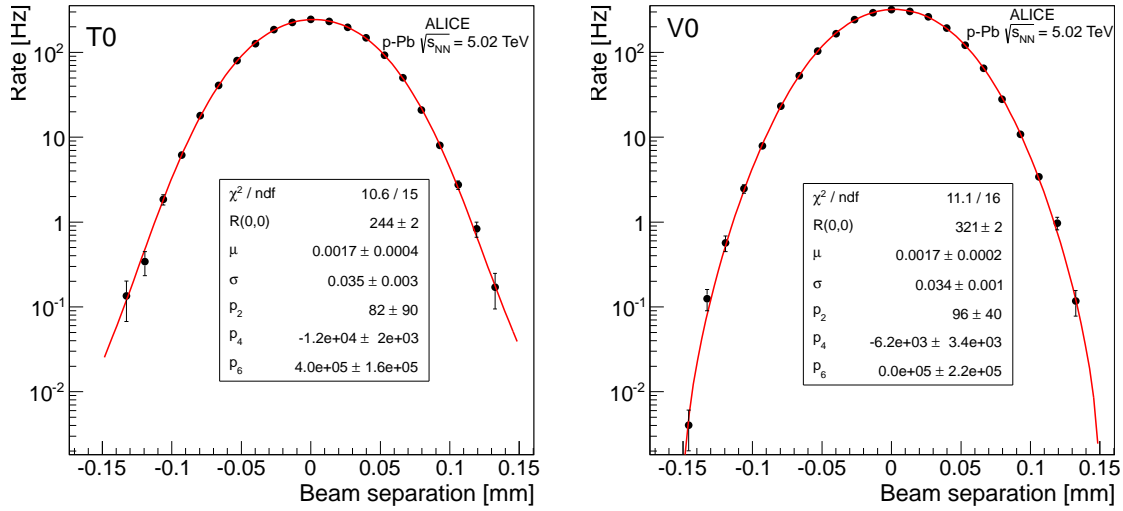
7

Fig. 6: (Colour online) Rates of the T0 (left) and V0 (right) reference process as a function of beam separation for one typical pair of colliding bunches in the first vertical p–Pb scan. The solid red curve is a fit according to equation 4.

into account in the evaluation of the systematic uncertainties.

The measured beam widths are corrected by a length-scale calibration factor. This correction aims to fine tune the conversion factor (known with limited precision) between the current in the steering magnets and the beam displacement. The calibration is performed in a dedicated run, where the two beams are moved simultaneously in the same direction in steps of equal size; the changes in the interaction vertex position provide a measurement of the actual beam displacement, which is used to extract a correction factor to the nominal displacement scale. The displacement of the vertex position is measured using data from the ALICE Inner Tracking System [13] and Time Projection Chamber [14]. This is shown in figure 8, left, for the horizontal length-scale calibration run. The correction factor is obtained as the slope parameter of a linear fit to the vertex displacement as a function of the nominal displacement (figure 8, right). Since this correction affects the global beam-displacement scale, all measured beam widths are multiplied by the correction factors 0.98±0.01 for the horizontal scale and 1.02±0.01 for the vertical scale.

The cross section for each colliding bunch pair and reference process is calculated according to equations 1 and 2 from the measured bunch intensities, beam widths and head-on rates. As there are two measured head-on rates per scan pair (one from the vertical and one from the horizontal scan), the arithmetic mean of the two is used, after checking that the two values are compatible within statistical uncertainties.

The measured cross sections (obtained with the numerical method) for the T0- and V0-based processes during the first scan of the p–Pb and Pb–p sessions are shown in figure 9 for all the colliding bunch pairs, as a function of the product of the colliding bunch intensities ($N_1 N_2$). No dependence of the results on $N_1 N_2$ is observed. Fluctuations beyond the statistical uncertainties are observed, and are more pronounced for the p–Pb session: such an effect is taken into account as a systematic uncertainty (see section 4).
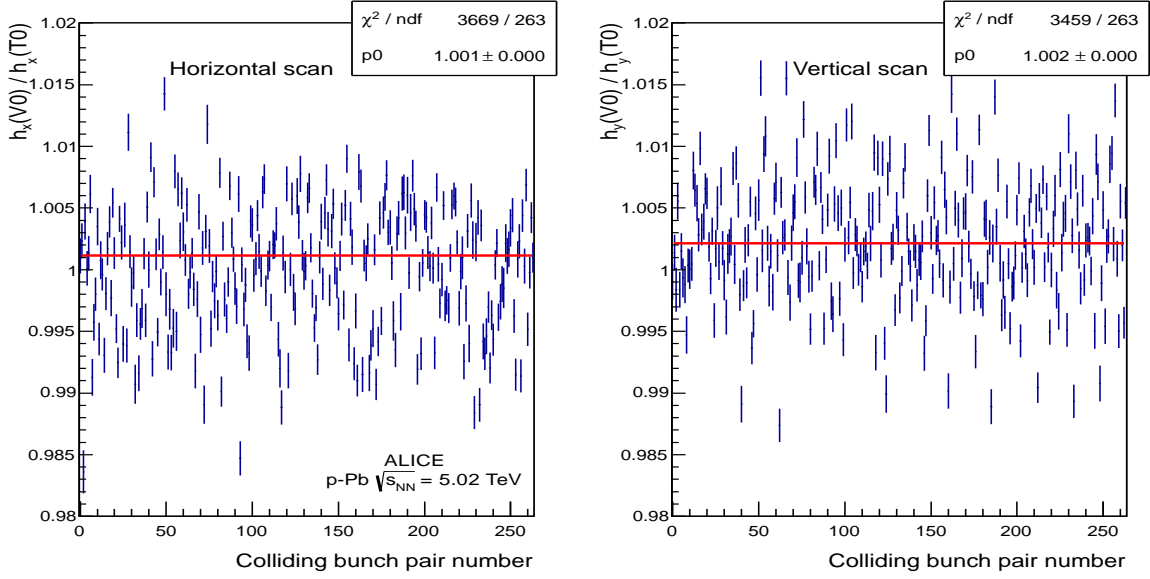
Fig. 7: (Colour online) Ratio between the horizontal (left) and vertical (right) effective beam widths obtained (via numerical method) with the T0 and V0 reference processes in the p–Pb scan session, as a function of the colliding bunch pair ID number. The solid red lines are zero-order-polynomial fits to the data.

Method	σ_{V0} [b]			σ_{T0} [b]		
	First scan	Second scan	Average	First scan	Second scan	Average
Numerical	2.087±0.001	2.098±0.001	**2.093±0.001**	1.590±0.001	1.598±0.001	**1.594±0.001**
Fit	2.087±0.001	2.099±0.001		1.596±0.001	1.599±0.001	

Table 1: Cross section for the V0- and T0-based reference process in two p–Pb vdM scans, as obtained with the numerical and fit methods. The weighted average between the numerical results of the two scans, retained as the final result, is also reported. The quoted uncertainties are statistical.

Method	σ_{V0} [b]			σ_{T0} [b]		
	First scan	Second scan	Average	First scan	Second scan	Average
Numerical	2.110±0.002	2.141±0.003	**2.122±0.002**	1.586±0.002	1.607±0.003	**1.594±0.002**
Fit	2.106±0.002	2.138±0.002		1.581±0.002	1.605±0.002	

Table 2: Cross section for the V0- and T0-based reference process in two Pb–p vdM scans, as obtained with the numerical and fit methods. The weighted average between the numerical results of the two scans, retained as the final result, is also reported. The quoted uncertainties are statistical.

4   Results and systematic uncertainties

For both processes and scan sessions the weighted average of results from all colliding bunch pairs is computed, for each scan and method. The results for all scans and methods are summarised in tables 1 and 2. The numerical and fit method agree to better than 0.4% for all scans. The numerical result is preferred, since it does not imply any assumption on the scan shape. For each session, the weighted average of the results of the two performed scans is retained as the final result. The differences between the two methods and between different scans in the same session are taken into account in the evaluation of the systematic uncertainties.

The sources of systematic uncertainty considered are listed below; unless otherwise specified, the quoted uncertainties apply to both the T0 and the V0 cross-section measurements.
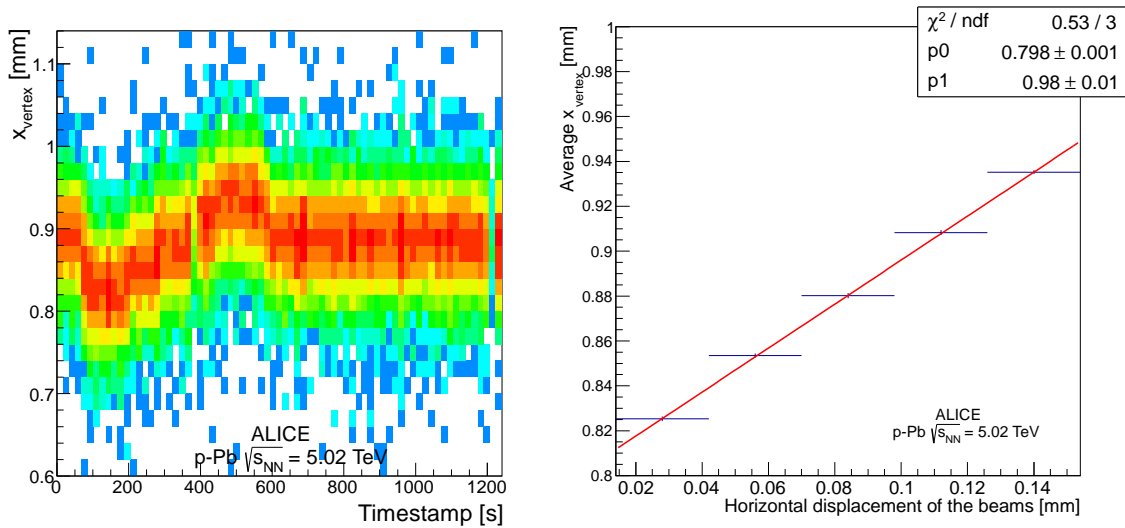
Fig. 8: (Colour online) Left: distribution of the horizontal interaction vertex coordinate as a function of time during the length-scale calibration run. The structure visible in the timestamp region between $\simeq$100 s and $\simeq$600 s corresponds to the beams being moved in five steps of 28 μm each. Right: average horizontal vertex coordinate as a function of the nominal horizontal beam displacement in the length-scale calibration run, with superimposed linear fit (solid red line).

- Bunch-by-bunch consistency: the RMS of the distribution of the cross section measured for all colliding bunch pairs (2% for the p–Pb scans and 1% for the Pb–p scans) is retained as a systematic uncertainty.

- Scan-to-scan consistency: the difference between the first and second scan in the same session (0.5% for the p–Pb scans and 1.5% for the Pb–p scans) is retained as a systematic uncertainty.

- Trigger dependence of the measured beam widths: as shown in figure 7 for the p–Pb session, discrepancies up to 1% are observed between the effective beam widths measured from T0 and V0 data, for both the horizontal and vertical directions. The same effect is observed in the Pb–p scan session. Since such discrepancies are beyond the statistical uncertainties, a 1.4% systematic uncertainty (1% for the vertical and 1% for the horizontal direction) is added to account for them.

- Background subtraction: in order to evaluate a possible bias arising from beam-beam events identified as beam-gas by the cut described in section 3, the analysis has been repeated by increasing the width of the window for beam-beam events from 8 to 14 ns: for the V0 cross section, a difference of 0.45% is found and added to the systematic uncertainty, for both configurations. The difference is negligible ($\ll 0.1\%$) for the T0 cross section.

- Method dependence, quantified via the maximum difference between the results obtained with the numerical and the fit method for each scan session: 0.4% for the p–Pb scans and 0.3% for the Pb–p scans.

- Beam centering: the measurement of $R(0,0)$ can be affected by a non-optimal alignment of the two beams in the head-on position. Such misalignment is quantified, for the x and y directions, via the μ parameter of equation 4. The value of μ is generally compatible with zero, with the exception of a few scans (the first horizontal and the second vertical p–Pb scan, the first horizontal Pb–p scan), where it reaches values up to 2.5 μm. The effect of such misalignment on the measured head-on rates was estimated using equation 4 and the obtained fit parameters: the resulting systematic uncertainty on the cross-section measurement is 0.3% (0.2%) for the p–Pb (Pb–p) configuration.
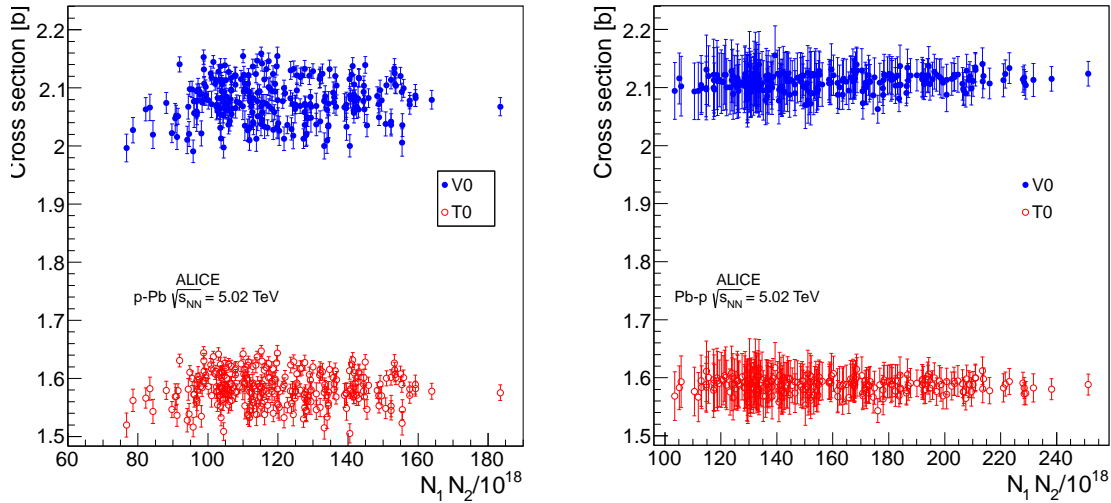
10

Fig. 9: (Colour online) Cross sections for the T0 and V0 processes measured in the first scan of the p–Pb (left) and Pb–p (right) sessions, as a function of the product of the intensities of the colliding bunch pair. The results are obtained with the numerical method. Only the statistical uncertainties are shown.

– Luminosity-decay correction: when varying the luminosity decay parameters within their uncertainties, a negligible ($< 0.1\%$) effect on the measured cross section is observed.

– Length-scale calibration: 1.5%, from the quadratic sum of the statistical uncertainties on the horizontal and vertical scale factors reported in section 3.

– Orbit drift: possible variations of the reference orbit during the scan may lead to a difference between the nominal and the real beam separation. In order to quantify a possible bias, the data from the LHC Beam Position Monitors (BPM) [15] in various locations along the ring are used to extrapolate, with the YASP steering program [16], the transverse coordinates of the reference orbit of the two beams at IP2, for each scan step. The (small) observed variations in the orbit are used to correct the separation values, and the cross section is re-calculated: a difference of 0.4% (0.1%) is found for the p–Pb (Pb–p) configuration results.

– Bunch intensity: the uncertainty on the DCCT beam-current measurement [17] is 0.46% (0.54%) for the p–Pb (Pb–p) scan session; given the very large fraction of colliding over circulating bunches, the uncertainty on the relative bunch populations has negligible effect on the cross section measurement [18].

– Ghost and satellite charge: the uncertainty on the LHCb ghost-charge measurement [11] propagates to an uncertainty of 0.1% (0.2%) on the p–Pb (Pb–p) cross-section measurement; the uncertainty in the LDM satellite-charge measurement [12] propagates to an uncertainty of 0.04% (0.1%) on the p–Pb (Pb–p) cross-section measurement.

– Dynamic β^*: due to their electric charge, the two colliding beams (de-)focus each other in a separation-dependent way, which alters the measured scan shape. Calculations [19] are used to estimate the variations of β^* with the separation, according to the prescription given in [20]: the effect on the measured cross section (partially correlated between the p–Pb and Pb–p sessions) is found to be $\leq 0.1\%$ for all p–Pb and Pb–p scans.

– Beam-beam deflection: due to their electric charge, the two beams exert a repulsive force upon each other [21]. Such repulsion results in a beam separation slightly different than its nominal

11

Uncertainty	p–Pp	Pb–p	Correlated between p–Pb and Pb–p
Bunch-by-bunch consistency	2%	1%	No
Scan-to-scan consistency	0.5%	1.5%	No
Length-scale calibration	1.5%	1.5%	Yes
Bunch size vs trigger	1.4%	1.4%	No
Background subtraction (V0 only)	0.5%	0.5%	Yes
Method dependence	0.4%	0.3%	No
Beam centering	0.3%	0.2%	No
Bunch intensity	0.5%	0.5%	No
Ghost charge	0.1%	0.2%	No
Satellite charge	<0.1%	0.1%	No
Orbit drift	0.4%	0.1%	No
Dynamic β^*	<0.1%	0.1%	Partially
Beam-beam deflection	0.2%	0.3%	Partially
Total on visible cross section	**3.0%**	**2.8%**	
V0- vs T0-based integrated luminosity	1%	1%	No
Total on integrated luminosity	**3.2%**	**3.0%**	

Table 3: Relative uncertainties on the measurement of the T0 and V0 reference process cross section in p–Pb and Pb–p collisions.

value. The variations of the beam separation are calculated using the MAD-X [22] code: the effect on the measured cross section (partially correlated between the p–Pb and Pb–p sessions) is found to be 0.2% (0.3%) for the p–Pb (Pb–p) scan, in the same direction for the two fills.

Summing in quadrature all the above-mentioned uncertainties (summarised in table 3), one gets a total systematic uncertainty of 3.0% for the p–Pb cross sections and 2.8% for the Pb–p cross sections. The uncertainty applies in the same way to the T0 and V0 cross sections, since the only non-common term is the background subtraction, which becomes negligible in the quadratic sum.

The final results for the p–Pb configuration are

$$\sigma_{V0} = 2.09\,\text{b} \pm 3.0\% = (2.09 \pm 0.06)\,\text{b}\,, \quad \sigma_{T0} = 1.59\,\text{b} \pm 3.0\% = (1.59 \pm 0.05)\,\text{b}$$

and those for the Pb–p configuration are

$$\sigma_{V0} = 2.12\,\text{b} \pm 2.8\% = (2.12 \pm 0.06)\,\text{b}\,, \quad \sigma_{T0} = 1.59\,\text{b} \pm 2.8\% = (1.59 \pm 0.05)\,\text{b}.$$

All uncertainties are systematic.

The length-scale calibration and background-subtraction uncertainties are fully correlated between the p–Pb and Pb–p results, leading to a total correlated uncertainty between the two measurements of 1.5% for T0 and 1.6% for V0.

The measured V0 cross section for Pb–p collisions is compatible, within uncertainties, with the visible cross section of (2.09±0.12) b measured by the LHCb experiment for an equivalent beam configuration in a similar pseudo-rapidity range ($3 < \eta < 5$) [23].

5   Comparison between V0- and T0-based luminosities

The visible cross sections measured in the vdM scans are used to determine the integrated luminosity for the data collected in the 2013 proton-lead run [24]. The luminosity is measured independently via the V0 or the T0 trigger counts, corrected for pileup and for background contamination in the same way as done for the vdM scan data, divided by the corresponding cross sections.

The data sample is divided in several smaller datasets (runs). The integrated luminosity corresponding to each run is computed using both reference processes, and the results are compared. Figure 10 shows the ratio of the integrated luminosity obtained with T0 to the one obtained with V0, as a function of the run number, for the p–Pb and Pb–p running modes. Although the overall agreement is satisfactory, fluctuations of about 1% around unity are seen in the run-by-run ratio; since these fluctuations are significantly larger than the tiny statistical uncertainties, a 1% additional systematic uncertainty is considered in the computation of the integrated luminosity uncertainty (table 3).
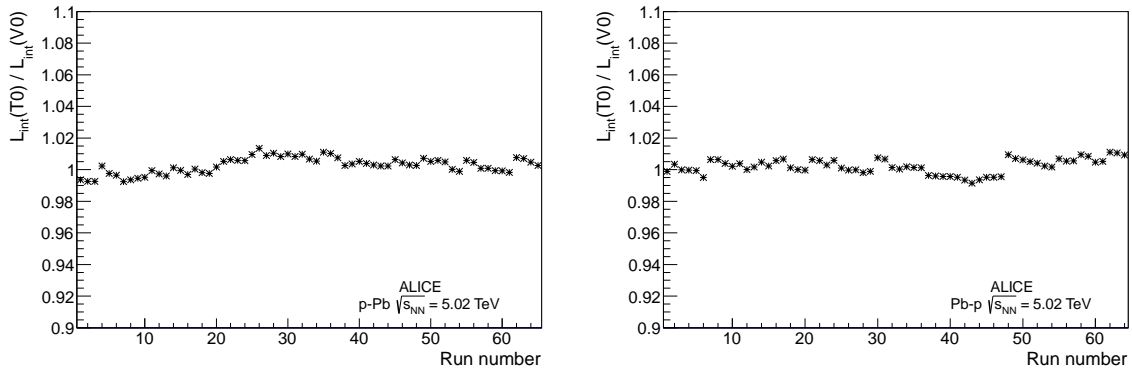

Fig. 10: Ratio of T0- to V0-based integrated luminosities as a function of run number for the p–Pb (left) and Pb–p (right) data taking. The tiny statistical uncertainties are covered by the data-point markers.

6   Measurement of the ZDC trigger cross section

The ALICE Zero Degree Calorimeter system (ZDC) [25] is composed of two neutron (ZN) and two proton (ZP) calorimeters, as well as two small electromagnetic calorimeters (ZEM). The two ZNs (ZNA and ZNC) are located on opposite sides of IP2, 112.5 m away from the interaction point. Each ZN is placed at zero degrees with respect to the ALICE z axis and is used to detect neutral particles at pseudorapidities $|\eta| > 8.8$. The ZNs were used to measure the cross section for neutron emission in Pb–Pb collisions at the LHC [26]. A similar study is foreseen in p–Pb collisions. For this purpose, data have been collected with a trigger condition requiring a signal in the ZN located on the Pb remnant side (i.e. ZNA for p–Pb, ZNC for Pb–p). In this paragraph, the measured T0 and V0 cross sections are used to determine indirectly the cross section for events satisfying such a trigger condition. Since the trigger condition is symmetric with respect to the swapping of the proton and lead beams, one expects the cross section to be the same in the p–Pb and Pb–p configurations. Thus, such a measurement provides a consistency check for the analysis of data from the two sessions.

The ZDC trigger cross section is calculated from the measured T0 and V0 cross sections, rescaled by the ratio of the ZDC trigger rate to the rate of the two reference processes, as measured during the two vdM scan sessions. All rates are corrected for background and pileup. The ratios and the resulting cross sections for the ZDC trigger are reported in table 4. The results obtained in the two fills are compatible within the uncorrelated uncertainties. The results obtained with T0 and V0 are also compatible. Thus, all results are combined to get

$$\sigma_{ZDC} = 2.21 \, \text{b} \pm 0.3\% \, (\text{stat}) \pm 2.4\% \, (\text{syst}) = 2.21 \, \text{b} \pm 0.01 \, \text{b} \, (\text{stat}) \pm 0.05 \, \text{b} \, (\text{syst}).$$

13

Configuration	Reference	$R_{ZDC}/R_{Reference}$	$\sigma_{ZDC} = \sigma_{Reference} \frac{R_{ZDC}}{R_{Reference}}$ [b]
p–Pb	T0	1.380±0.014 (stat.)	2.20±0.02 (stat.) ± 0.06 (syst. uncorr.) ±0.03 (syst. corr.)
p–Pb	V0	1.046±0.012 (stat.)	2.19±0.02 (stat.) ± 0.06 (syst. uncorr.) ±0.03 (syst. corr.)
Pb–p	T0	1.404±0.005 (stat.)	2.24±0.01 (stat.) ± 0.05 (syst. uncorr.) ±0.03 (syst. corr.)
Pb–p	V0	1.050±0.004 (stat.)	2.23±0.01 (stat.) ± 0.05 (syst. uncorr.) ±0.03 (syst. corr.)

Table 4: Ratio of the ZDC to the reference process rates and ZDC cross sections resulting from such ratios, for all reference processes and beam configurations. The uncertainties are split into correlated and uncorrelated components between the p–Pb and the Pb–p sessions.

7   Conclusions

Van der Meer scans were done for proton-lead collisions at $\sqrt{s_{NN}} = 5.02$ TeV at the LHC. The cross section was measured for two reference processes, based on particle detection by the T0 ($4.6 < \eta < 4.9$ and $-3.3 < \eta < -3.0$) and V0 ($2.8 < \eta < 5.1$ and $-3.7 < \eta < -1.7$) detectors. For the p–Pb configuration (proton beam travelling clockwise), the measured cross sections are $\sigma_{V0} = 2.09$ b $\pm$ 3.0% (syst) and $\sigma_{T0} = 1.59$ b $\pm$ 3.0% (syst). For the Pb–p configuration (proton beam travelling counter-clockwise), the measured cross sections are $\sigma_{V0} = 2.12$ b $\pm$ 2.8% (syst) and $\sigma_{T0} = 1.59$ b $\pm$ 2.8% (syst). The two reference processes were independently used for the luminosity determination in the 2013 proton-lead run at the LHC. The luminosities measured via the two processes differ by at most 1% throughout the whole data-taking period; with such value quadratically added to the reference process cross section uncertainties, a total uncertainty on the integrated luminosity measurement of 3.2% (3.0%) for the p–Pb (Pb–p) configuration is obtained. Finally, the measured reference cross sections were used to indirectly determine the cross section for a third, configuration-independent, reference process, based on neutron detection by the Zero Degree Calorimeter: $\sigma_{ZDC} = 2.21$ b $\pm$ 0.3% (stat) $\pm$ 2.4% (syst).

8   Acknowledgements

References

[1] K. Aamodt et al. [ALICE Collaboration], JINST 3 S08002 (2008).

[2] S. van der Meer, CERN-ISR-PO-68-31 (1968).

[3] V. Balagura, NIM A 654 634 (2011).

[4] B. Abelev et al. [ALICE Collaboration], arXiv:1402.4476 [nucl-ex] (2014).

[5] T. Malkiewicz et al., IJP 85 965 (2011).

[6] E. Abbas et al. [ALICE Collaboration], JINST 8 P10016 (2013).

[7] B. Abelev et al. [ALICE Collaboration], PRL 110 032301 (2013).

[8] M. Schaumann and J.M. Jowett, in Proceedings of IPAC 2013 (TUPFI025), Shanghai, China (2013).

[9] J.J. Gras et al., CERN-ATS-2011-063 (2011).

[10] A. Alici et al., CERN-ATS-Note-2012-029 PERF (2012).

[11] C. Barschel, Ph.D. Thesis, RWTH Aachen University (2013).

[12] A. Boccardi et al., CERN-ATS-Note-2013-034 TECH (2013).

[13] K. Aamodt et al. [ALICE Collaboration], JINST 5 P03003 (2010).

[14] J. Alme et al., NIM A 622 316 (2010).

[15] E. Calvo et al, in Proceedings of DIPAC 2003, Mainz, Germany (2003)
     http://accelconf.web.cern.ch/accelconf/d03/html/auth0032.html.

[16] J. Wenninger, CERN-LHC-Performance-Note-005 (2009).

[17] C. Barschel et al., CERN-ATS-Note-2012-026 PERF (2012) and private communication within the
     LHC Luminosity Calibration and Measurement Working Group.

[18] G. Anders et al., CERN-ATS-Note-2012-028 PERF (2012).

[19] W. Herr, in Proceedings of the LHC Lumi Days 2012, Geneva, Switzerland (2012)
     http://indico.cern.ch/event/162948/session/4/contribution/27/material/paper/.

[20] G. Aad et al. [ATLAS Collaboration], EPJ C 73:2518 (2013).

[21] W. Kozanecki et al., CERN-ACC-NOTE-2013-0006 (2013).

[22] CERN Accelerator Beam Physics Group, MAD-Methodical Accelerator Design
     http://mad.web.cern.ch/mad/.

[23] M. Schmelling et al. [LHCb Collaboration], LHCb-CONF-2012-034 (2012).

[24] B. Abelev et al. [ALICE Collaboration], JHEP 1402 073 (2014).

[25] A. De Falco et al., NIM A 595 267 (2008).

[26] B. Abelev et al. [ALICE Collaboration], PRL 109 252302 (2012).

A   The ALICE Collaboration

B. Abelev[69], J. Adam[37], D. Adamová[77], M.M. Aggarwal[81], M. Agnello[105 ,88], A. Agostinelli[26], N. Agrawal[44], Z. Ahammed[124], N. Ahmad[18], I. Ahmed[15], S.U. Ahn[62], S.A. Ahn[62], I. Aimo[105 ,88], S. Aiola[129], M. Ajaz[15], A. Akindinov[53], S.N. Alam[124], D. Aleksandrov[94], B. Alessandro[105], D. Alexandre[96], A. Alici[12 ,99], A. Alkin[3], J. Alme[35], T. Alt[39], S. Altinpinar[17], I. Altsybeev[123], C. Alves Garcia Prado[113], C. Andrei[72 ,72], A. Andronic[91], V. Anguelov[87], J. Anielski[49], T. Antičić[92], F. Antinori[102], P. Antonioli[99], L. Aphecetche[107], H. Appelshäuser[48], N. Arbor[65], S. Arcelli[26], N. Armesto[16], R. Arnaldi[105], T. Aronsson[129], I.C. Arsene[91], M. Arslandok[48], A. Augustinus[34], R. Averbeck[91], T.C. Awes[78], M.D. Azmi[83], M. Bach[39], A. Badalà[101], Y.W. Baek[64 ,40], S. Bagnasco[105], R. Bailhache[48], R. Bala[84], A. Baldisseri[14], F. Baltasar Dos Santos Pedrosa[34], R.C. Baral[56], R. Barbera[27], F. Barile[31], G.G. Barnaföldi[128], L.S. Barnby[96], V. Barret[64], J. Bartke[110], M. Basile[26], N. Bastid[64], S. Basu[124], B. Bathen[49], G. Batigne[107], B. Batyunya[61], P.C. Batzing[21], C. Baumann[48], I.G. Bearden[74], H. Beck[48], C. Bedda[88], N.K. Behera[44], I. Belikov[50], F. Bellini[26], R. Bellwied[115], E. Belmont-Moreno[59], R. Belmont III[127], G. Bencedi[128], S. Beole[25], I. Berceanu[72], A. Bercuci[72], Y. Berdnikov[ii,79], D. Berenyi[128], M.E. Berger[86], R.A. Bertens[52], D. Berzano[25], L. Betev[34], A. Bhasin[84], I.R. Bhat[84], A.K. Bhati[81], B. Bhattacharjee[41], J. Bhom[120], L. Bianchi[25], N. Bianchi[66], C. Bianchin[52], J. Bielčík[37], J. Bielčíková[77], A. Bilandzic[74], S. Bjelogrlic[52], F. Blanco[10], D. Blau[94], C. Blume[48], F. Bock[87 ,68], A. Bogdanov[70], H. Bøggild[74], M. Bogolyubsky[106], F.V. Böhmer[86], L. Boldizsár[128], M. Bombara[38], J. Book[48], H. Borel[14], A. Borissov[90 ,127], F. Bossú[60], M. Botje[75], E. Botta[25], S. Böttger[47 ,47], P. Braun-Munzinger[91], M. Bregant[113], T. Breitner[47], T.A. Broker[48], T.A. Browning[89], M. Broz[37], E. Bruna[105], G.E. Bruno[31], D. Budnikov[93], H. Buesching[48], S. Bufalino[105], P. Buncic[34], O. Busch[87], Z. Buthelezi[60], D. Caffarri[28], X. Cai[7], H. Caines[129], L. Calero Diaz[66], A. Caliva[52], E. Calvo Villar[97], P. Camerini[24], F. Carena[34], W. Carena[34], J. Castillo Castellanos[14], E.A.R. Casula[23], V. Catanescu[72], C. Cavicchioli[34], C. Ceballos Sanchez[9], J. Cepila[37], P. Cerello[105], B. Chang[116], S. Chapeland[34], J.L. Charvet[14], S. Chattopadhyay[124], S. Chattopadhyay[95], V. Chelnokov[3], M. Cherney[80], C. Cheshkov[122], B. Cheynis[122], V. Chibante Barroso[34], D.D. Chinellato[115], P. Chochula[34], M. Chojnacki[74], S. Choudhury[124], P. Christakoglou[75], C.H. Christensen[74], P. Christiansen[32], T. Chujo[120], S.U. Chung[90], C. Cicalo[100], L. Cifarelli[12 ,26], F. Cindolo[99], J. Cleymans[83], F. Colamaria[31], D. Colella[31], A. Collu[23], M. Colocci[26], G. Conesa Balbastre[65], Z. Conesa del Valle[46], M.E. Connors[129], J.G. Contreras[11], T.M. Cormier[127], Y. Corrales Morales[25], P. Cortese[30], I. Cortés Maldonado[2], M.R. Cosentino[113], F. Costa[34], P. Crochet[64], R. Cruz Albino[11], E. Cuautle[58], L. Cunqueiro[66], A. Dainese[102], R. Dang[7], A. Danu[57], D. Das[95], I. Das[46], K. Das[95], S. Das[4], A. Dash[114], S. Dash[44], S. De[124], H. Delagrange[107 ,i], A. Deloff[71], E. Dénes[128], G. D'Erasmo[31], A. De Caro[29 ,12], G. de Cataldo[98], J. de Cuveland[39], A. De Falco[23], D. De Gruttola[29 ,12], N. De Marco[105], S. De Pasquale[29], R. de Rooij[52], M.A. Diaz Corchero[10], T. Dietel[49], P. Dillenseger[48], R. Divià[34], D. Di Bari[31], S. Di Liberto[103], A. Di Mauro[34], P. Di Nezza[66], Ø. Djuvsland[17], A. Dobrin[52], T. Dobrowolski[71], D. Domenicis Gimenez[113], B. Dönigus[48], O. Dordic[21], S. Dørheim[86], A.K. Dubey[124], A. Dubla[52], L. Ducroux[122], P. Dupieux[64], A.K. Dutta Majumdar[95], R.J. Ehlers[129], D. Elia[98], H. Engel[47], B. Erazmus[34 ,107], H.A. Erdal[35], D. Eschweiler[39], B. Espagnon[46], M. Esposito[34], M. Estienne[107], S. Esumi[120], D. Evans[96], S. Evdokimov[106], D. Fabris[102], J. Faivre[65], D. Falchieri[26], A. Fantoni[66], M. Fasel[87], D. Fehlker[17], L. Feldkamp[49], D. Felea[57], A. Feliciello[105], G. Feofilov[123], J. Ferencei[77], A. Fernández Téllez[2], E.G. Ferreiro[16], A. Ferretti[25], A. Festanti[28], J. Figiel[110], M.A.S. Figueredo[117], S. Filchagin[93], D. Finogeev[51], F.M. Fionda[31], E.M. Fiore[31], E. Floratos[82], M. Floris[34], S. Foertsch[60], P. Foka[91], S. Fokin[94], E. Fragiacomo[104], A. Francescon[34 ,28], U. Frankenfeld[91], U. Fuchs[34], C. Furget[65], M. Fusco Girard[29], J.J. Gaardhøje[74], M. Gagliardi[25], A.M. Gago[97], M. Gallio[25], D.R. Gangadharan[19], P. Ganoti[78], C. Garabatos[91], E. Garcia-Solis[13], C. Gargiulo[34], I. Garishvili[69], J. Gerhard[39], M. Germain[107], A. Gheata[34], M. Gheata[34 ,57], B. Ghidini[31], P. Ghosh[124], S.K. Ghosh[4], P. Gianotti[66], P. Giubellino[34], E. Gladysz-Dziadus[110], P. Glässel[87], A. Gomez Ramirez[47], P. González-Zamora[10], S. Gorbunov[39], L. Görlich[110], S. Gotovac[109], L.K. Graczykowski[126], A. Grelli[52], A. Grigoras[34], C. Grigoras[34], V. Grigoriev[70], A. Grigoryan[1], S. Grigoryan[61], B. Grinyov[3], N. Grion[104], J.F. Grosse-Oetringhaus[34], J.-Y. Grossiord[122], R. Grosso[34], F. Guber[51], R. Guernane[65], B. Guerzoni[26], M. Guilbaud[122], K. Gulbrandsen[74], H. Gulkanyan[1], M. Gumbo[83], T. Gunji[119], A. Gupta[84], R. Gupta[84], K. H. Khan[15], R. Haake[49], Ø. Haaland[17], C. Hadjidakis[46], M. Haiduc[57], H. Hamagaki[119], G. Hamar[128], L.D. Hanratty[96], A. Hansen[74], J.W. Harris[129], H. Hartmann[39], A. Harton[13], D. Hatzifotiadou[99], S. Hayashi[119], S.T. Heckel[48], M. Heide[49], H. Helstrup[35], A. Herghelegiu[72 ,72], G. Herrera Corral[11], B.A. Hess[33], K.F. Hetland[35], B. Hippolyte[50], J. Hladky[55], P. Hristov[34], M. Huang[17], T.J. Humanic[19], D. Hutter[39], D.S. Hwang[20], R. Ilkaev[93], I. Ilkiv[71], M. Inaba[120], G.M. Innocenti[25], C. Ionita[34], M. Ippolitov[94], M. Irfan[18], M. Ivanov[91], V. Ivanov[79], A. Jachołkowski[27], P.M. Jacobs[68], C. Jahnke[113], H.J. Jang[62], M.A. Janik[126], P.H.S.Y. Jayarathna[115], S. Jena[115],

R.T. Jimenez Bustamante[58] , P.G. Jones[96] , H. Jung[40] , A. Jusko[96] , V. Kadyshevskiy[61] , S. Kalcher[39] , P. Kalinak[54 ,54] , A. Kalweit[34] , J. Kamin[48] , J.H. Kang[130] , V. Kaplin[70] , S. Kar[124] , A. Karasu Uysal[63] , O. Karavichev[51] , T. Karavicheva[51] , E. Karpechev[51] , U. Kebschull[47] , R. Keidel[131] , M.M. Khan[iii,18] , P. Khan[95] , S.A. Khan[124] , A. Khanzadeev[79] , Y. Kharlov[106] , B. Kileng[35] , B. Kim[130] , D.W. Kim[62 ,40] , D.J. Kim[116] , J.S. Kim[40] , M. Kim[40] , M. Kim[130] , S. Kim[20] , T. Kim[130] , S. Kirsch[39] , I. Kisel[39] , S. Kiselev[53] , A. Kisiel[126] , G. Kiss[128] , J.L. Klay[6] , J. Klein[87] , C. Klein-Bösing[49] , A. Kluge[34] , M.L. Knichel[91] , A.G. Knospe[111] , C. Kobdaj[34 ,108] , M.K. Köhler[91] , T. Kollegger[39] , A. Kolojvari[123] , V. Kondratiev[123] , N. Kondratyeva[70] , A. Konevskikh[51] , V. Kovalenko[123] , M. Kowalski[110] , S. Kox[65] , G. Koyithatta Meethaleveedu[44] , J. Kral[116] , I. Králik[54] , F. Kramer[48] , A. Kravčáková[38] , M. Krelina[37] , M. Kretz[39] , M. Krivda[96 ,54] , F. Krizek[77] , E. Kryshen[34] , M. Krzewicki[91] , V. Kučera[77] , Y. Kucheriaev[94 ,i] , T. Kugathasan[34] , C. Kuhn[50] , P.G. Kuijer[75] , I. Kulakov[48] , J. Kumar[44] , P. Kurashvili[71] , A. Kurepin[51] , A.B. Kurepin[51] , A. Kuryakin[93] , S. Kushpil[77] , M.J. Kweon[87] , Y. Kwon[130] , P. Ladron de Guevara[58] , C. Lagana Fernandes[113] , I. Lakomov[46] , R. Langoy[125] , C. Lara[47] , A. Lardeux[107] , A. Lattuca[25] , S.L. La Pointe[52] , P. La Rocca[27] , R. Lea[24 ,24] , G.R. Lee[96] , I. Legrand[34] , J. Lehnert[48] , R.C. Lemmon[76] , V. Lenti[98] , E. Leogrande[52] , M. Leoncino[25] , I. León Monzón[112] , P. Lévai[128] , S. Li[7 ,64] , J. Lien[125] , R. Lietava[96] , S. Lindal[21] , V. Lindenstruth[39] , C. Lippmann[91] , M.A. Lisa[19] , H.M. Ljunggren[32] , D.F. Lodato[52] , P.I. Loenne[17] , V.R. Loggins[127] , V. Loginov[70] , D. Lohner[87] , C. Loizides[68] , X. Lopez[64] , E. López Torres[9] , X.-G. Lu[87] , P. Luettig[48] , M. Lunardon[28] , G. Luparello[52] , C. Luzzi[34] , R. Ma[129] , A. Maevskaya[51] , M. Mager[34] , D.P. Mahapatra[56] , S.M. Mahmood[21] , A. Maire[87] , R.D. Majka[129] , M. Malaev[79] , I. Maldonado Cervantes[58] , L. Malinina[iv,61] , D. Mal'Kevich[53] , P. Malzacher[91] , A. Mamonov[93] , L. Manceau[105] , V. Manko[94] , F. Manso[64] , V. Manzari[98] , M. Marchisone[64 ,25] , J. Mareš[55] , G.V. Margagliotti[24] , A. Margotti[99] , A. Marín[91] , C. Markert[111] , M. Marquard[48] , I. Martashvili[118] , N.A. Martin[91] , P. Martinengo[34] , M.I. Martínez[2] , G. Martínez García[107] , J. Martin Blanco[107] , Y. Martynov[3] , A. Mas[107] , S. Masciocchi[91] , M. Masera[25] , A. Masoni[100] , L. Massacrier[107] , A. Mastroserio[31] , A. Matyja[110] , C. Mayer[110] , J. Mazer[118] , M.A. Mazzoni[103] , F. Meddi[22] , A. Menchaca-Rocha[59] , J. Mercado Pérez[87] , M. Meres[36] , Y. Miake[120] , K. Mikhaylov[61 ,53] , L. Milano[34] , J. Milosevic[v,21] , A. Mischke[52] , A.N. Mishra[45] , D. Miśkowiec[91] , J. Mitra[124] , C.M. Mitu[57] , J. Mlynarz[127] , N. Mohammadi[52] , B. Mohanty[73 ,124] , L. Molnar[50] , L. Montaño Zetina[11] , E. Montes[10] , M. Morando[28] , D.A. Moreira De Godoy[113] , S. Moretto[28] , A. Morreale[116] , A. Morsch[34] , V. Muccifora[66] , E. Mudnic[109] , D. Mühlheim[49] , S. Muhuri[124] , M. Mukherjee[124] , H. Müller[34] , M.G. Munhoz[113] , S. Murray[83] , L. Musa[34] , J. Musinsky[54] , B.K. Nandi[44] , R. Nania[99] , E. Nappi[98] , C. Nattrass[118] , K. Nayak[73] , T.K. Nayak[124] , S. Nazarenko[93] , A. Nedosekin[53] , M. Nicassio[91] , M. Niculescu[34 ,57] , B.S. Nielsen[74] , S. Nikolaev[94] , S. Nikulin[94] , V. Nikulin[79] , B.S. Nilsen[80] , F. Noferini[12 ,99] , P. Nomokonov[61] , G. Nooren[52] , A. Nyanin[94] , J. Nystrand[17] , H. Oeschler[87] , S. Oh[129] , S.K. Oh[vi,40] , A. Okatan[63] , L. Olah[128] , J. Oleniacz[126] , A.C. Oliveira Da Silva[113] , J. Onderwaater[91] , C. Oppedisano[105] , A. Ortiz Velasquez[32] , A. Oskarsson[32] , J. Otwinowski[91] , K. Oyama[87] , P. Sahoo[45] , Y. Pachmayer[87] , M. Pachr[37] , P. Pagano[29] , G. Paić[58] , F. Painke[39] , C. Pajares[16] , S.K. Pal[124] , A. Palmeri[101] , D. Pant[44] , V. Papikyan[1] , G.S. Pappalardo[101] , P. Pareek[45] , W.J. Park[91] , S. Parmar[81] , A. Passfeld[49] , D.I. Patalakha[106] , V. Paticchio[98] , B. Paul[95] , T. Pawlak[126] , T. Peitzmann[52] , H. Pereira Da Costa[14] , E. Pereira De Oliveira Filho[113] , D. Peresunko[94] , C.E. Pérez Lara[75] , A. Pesci[99] , V. Peskov[48] , Y. Pestov[5] , V. Petráček[37] , M. Petran[37] , M. Petris[72] , M. Petrovici[72] , C. Petta[27] , S. Piano[104] , M. Pikna[36] , P. Pillot[107] , O. Pinazza[99 ,34] , L. Pinsky[115] , D.B. Piyarathna[115] , M. Płoskoń[68] , M. Planinic[121 ,92] , J. Pluta[126] , S. Pochybova[128] , P.L.M. Podesta-Lerma[112] , M.G. Poghosyan[34] , E.H.O. Pohjoisaho[42] , B. Polichtchouk[106] , N. Poljak[92] , A. Pop[72] , S. Porteboeuf-Houssais[64] , J. Porter[68] , B. Potukuchi[84] , S.K. Prasad[127] , R. Preghenella[99 ,12] , F. Prino[105] , C.A. Pruneau[127] , I. Pshenichnov[51] , G. Puddu[23] , P. Pujahari[127] , V. Punin[93] , J. Putschke[127] , H. Qvigstad[21] , A. Rachevski[104] , S. Raha[4] , J. Rak[116] , A. Rakotozafindrabe[14] , L. Ramello[30] , R. Raniwala[85] , S. Raniwala[85] , S.S. Räsänen[42] , B.T. Rascanu[48] , D. Rathee[81] , A.W. Rauf[15] , V. Razazi[23] , K.F. Read[118] , J.S. Real[65] , K. Redlich[vii,71] , R.J. Reed[129] , A. Rehman[17] , P. Reichelt[48] , M. Reicher[52] , F. Reidt[34] , R. Renfordt[48] , A.R. Reolon[66] , A. Reshetin[51] , F. Rettig[39] , J.-P. Revol[34] , K. Reygers[87] , V. Riabov[79] , R.A. Ricci[67] , T. Richert[32] , M. Richter[21] , P. Riedler[34] , W. Riegler[34] , F. Riggi[27] , A. Rivetti[105] , E. Rocco[52] , M. Rodríguez Cahuantzi[2] , A. Rodriguez Manso[75] , K. Røed[21] , E. Rogochaya[61] , S. Rohni[84] , D. Rohr[39] , D. Röhrich[17] , R. Romita[76] , F. Ronchetti[66] , P. Rosnet[64] , A. Rossi[34] , F. Roukoutakis[82] , A. Roy[45] , C. Roy[50] , P. Roy[95] , A.J. Rubio Montero[10] , R. Rui[24] , R. Russo[25] , E. Ryabinkin[94] , Y. Ryabov[79] , A. Rybicki[110] , S. Sadovsky[106] , K. Šafařík[34] , B. Sahlmuller[48] , R. Sahoo[45] , P.K. Sahu[56] , J. Saini[124] , S. Sakai[68] , C.A. Salgado[16] , J. Salzwedel[19] , S. Sambyal[84] , V. Samsonov[79] , X. Sanchez Castro[50] , F.J. Sánchez Rodríguez[112] , L. Šándor[54] , A. Sandoval[59] , M. Sano[120] , G. Santagati[27] , D. Sarkar[124] , E. Scapparone[99] , F. Scarlassara[28] , R.P. Scharenberg[89] , C. Schiaua[72] , R. Schicker[87] , C. Schmidt[91] , H.R. Schmidt[33] , S. Schuchmann[48] , J. Schukraft[34] , M. Schulc[37] , T. Schuster[129] , Y. Schutz[107 ,34] , K. Schwarz[91] , K. Schweda[91] , G. Scioli[26] , E. Scomparin[105] , R. Scott[118] , G. Segato[28] , J.E. Seger[80] ,

Y. Sekiguchi[119] , I. Selyuzhenkov[91] , J. Seo[90] , E. Serradilla[10 ,59] , A. Sevcenco[57] , A. Shabetai[107] ,
G. Shabratova[61] , R. Shahoyan[34] , A. Shangaraev[106] , N. Sharma[118] , S. Sharma[84] , K. Shigaki[43] , K. Shtejer[25] ,
Y. Sibiriak[94] , S. Siddhanta[100] , T. Siemiarczuk[71] , D. Silvermyr[78] , C. Silvestre[65] , G. Simatovic[121] ,
R. Singaraju[124] , R. Singh[84] , S. Singha[124 ,73] , V. Singhal[124] , B.C. Sinha[124] , T. Sinha[95] , B. Sitar[36] , M. Sitta[30] ,
T.B. Skaali[21] , K. Skjerdal[17] , M. Slupecki[116] , N. Smirnov[129] , R.J.M. Snellings[52] , C. Søgaard[32] , R. Soltz[69] ,
J. Song[90] , M. Song[130] , F. Soramel[28] , S. Sorensen[118] , M. Spacek[37] , I. Sputowska[110] ,
M. Spyropoulou-Stassinaki[82] , B.K. Srivastava[89] , J. Stachel[87] , I. Stan[57] , G. Stefanek[71] , M. Steinpreis[19] ,
E. Stenlund[32] , G. Steyn[60] , J.H. Stiller[87] , D. Stocco[107] , M. Stolpovskiy[106] , P. Strmen[36] , A.A.P. Suaide[113] ,
T. Sugitate[43] , C. Suire[46] , M. Suleymanov[15] , R. Sultanov[53] , M. Šumbera[77] , T. Susa[92] , T.J.M. Symons[68] ,
A. Szabo[36] , A. Szanto de Toledo[113] , I. Szarka[36] , A. Szczepankiewicz[34] , M. Szymanski[126] , J. Takahashi[114] ,
M.A. Tangaro[31] , J.D. Tapia Takaki[·viii,46] , A. Tarantola Peloni[48] , A. Tarazona Martinez[34] , M.G. Tarzila[72] ,
A. Tauro[34] , G. Tejeda Muñoz[2] , A. Telesca[34] , C. Terrevoli[23] , J. Thäder[91] , D. Thomas[52] , R. Tieulent[122] ,
A.R. Timmins[115] , A. Toia[102] , H. Torii[119] , V. Trubnikov[3] , W.H. Trzaska[116] , T. Tsuji[119] , A. Tumkin[93] ,
R. Turrisi[102] , T.S. Tveter[21] , J. Ulery[48] , K. Ullaland[17] , A. Uras[122] , G.L. Usai[23] , M. Vajzer[77] , M. Vala[54 ,61] ,
L. Valencia Palomo[64 ,46] , S. Vallero[87] , P. Vande Vyvre[34] , L. Vannucci[67] , J. Van Der Maarel[52] ,
J.W. Van Hoorne[34] , M. van Leeuwen[52] , A. Vargas[2] , M. Vargyas[116] , R. Varma[44] , M. Vasileiou[82] , A. Vasiliev[94] ,
V. Vechernin[123] , M. Veldhoen[52] , A. Velure[17] , M. Venaruzzo[24 ,67] , E. Vercellin[25] , S. Vergara Limón[2] ,
R. Vernet[8] , M. Verweij[127] , L. Vickovic[109] , G. Viesti[28] , J. Viinikainen[116] , Z. Vilakazi[60] , O. Villalobos Baillie[96] ,
A. Vinogradov[94] , L. Vinogradov[123] , Y. Vinogradov[93] , T. Virgili[29] , Y.P. Viyogi[124] , A. Vodopyanov[61] ,
M.A. Völkl[87] , K. Voloshin[53] , S.A. Voloshin[127] , G. Volpe[34] , B. von Haller[34] , I. Vorobyev[123] , D. Vranic[91 ,34] ,
J. Vrláková[38] , B. Vulpescu[64] , A. Vyushin[93] , B. Wagner[17] , J. Wagner[91] , V. Wagner[37] , M. Wang[7 ,107] ,
Y. Wang[87] , D. Watanabe[120] , M. Weber[115] , J.P. Wessels[49] , U. Westerhoff[49] , J. Wiechula[33] , J. Wikne[21] ,
M. Wilde[49] , G. Wilk[71] , J. Wilkinson[87] , M.C.S. Williams[99] , B. Windelband[87] , M. Winn[87] , C. Xiang[7] ,
C.G. Yaldo[127] , Y. Yamaguchi[119] , H. Yang[52] , P. Yang[7] , S. Yang[17] , S. Yano[43] , S. Yasnopolskiy[94] , J. Yi[90] ,
Z. Yin[7] , I.-K. Yoo[90] , I. Yushmanov[94] , V. Zaccolo[74] , C. Zach[37] , A. Zaman[15] , C. Zampolli[99] , S. Zaporozhets[61] ,
A. Zarochentsev[123] , P. Závada[55] , N. Zaviyalov[93] , H. Zbroszczyk[126] , I.S. Zgura[57] , M. Zhalov[79] , H. Zhang[7] ,
X. Zhang[68 ,7] , Y. Zhang[7] , C. Zhao[21] , N. Zhigareva[53] , D. Zhou[7] , F. Zhou[7] , Y. Zhou[52] , Zhou, Zhuo[17] , H. Zhu[7] ,
J. Zhu[7] , X. Zhu[7] , A. Zichichi[12 ,26] , A. Zimmermann[87] , M.B. Zimmermann[34 ,49] , G. Zinovjev[3] ,
Y. Zoccarato[122] , M. Zyzak[48]

Affiliation notes

[i] Deceased
[ii] Also at: St. Petersburg State Polytechnical University
[iii] Also at: Department of Applied Physics, Aligarh Muslim University, Aligarh, India
[iv] Also at: M.V. Lomonosov Moscow State University, D.V. Skobeltsyn Institute of Nuclear Physics, Moscow, Russia
[v] Also at: University of Belgrade, Faculty of Physics and "Vinča" Institute of Nuclear Sciences, Belgrade, Serbia
[vi] Permanent Address: Permanent Address: Konkuk University, Seoul, Korea
[vii] Also at: Institute of Theoretical Physics, University of Wroclaw, Wroclaw, Poland
[viii] Also at: University of Kansas, Lawrence, KS, United States

Collaboration Institutes

[1] A.I. Alikhanyan National Science Laboratory (Yerevan Physics Institute) Foundation, Yerevan, Armenia
[2] Benemérita Universidad Autónoma de Puebla, Puebla, Mexico
[3] Bogolyubov Institute for Theoretical Physics, Kiev, Ukraine
[4] Bose Institute, Department of Physics and Centre for Astroparticle Physics and Space Science (CAPSS), Kolkata, India
[5] Budker Institute for Nuclear Physics, Novosibirsk, Russia
[6] California Polytechnic State University, San Luis Obispo, CA, United States
[7] Central China Normal University, Wuhan, China
[8] Centre de Calcul de l'IN2P3, Villeurbanne, France
[9] Centro de Aplicaciones Tecnológicas y Desarrollo Nuclear (CEADEN), Havana, Cuba
[10] Centro de Investigaciones Energéticas Medioambientales y Tecnológicas (CIEMAT), Madrid, Spain
[11] Centro de Investigación y de Estudios Avanzados (CINVESTAV), Mexico City and Mérida, Mexico

[12] Centro Fermi - Museo Storico della Fisica e Centro Studi e Ricerche "Enrico Fermi", Rome, Italy

[13] Chicago State University, Chicago, USA

[14] Commissariat à l'Energie Atomique, IRFU, Saclay, France

[15] COMSATS Institute of Information Technology (CIIT), Islamabad, Pakistan

[16] Departamento de Física de Partículas and IGFAE, Universidad de Santiago de Compostela, Santiago de Compostela, Spain

[17] Department of Physics and Technology, University of Bergen, Bergen, Norway

[18] Department of Physics, Aligarh Muslim University, Aligarh, India

[19] Department of Physics, Ohio State University, Columbus, OH, United States

[20] Department of Physics, Sejong University, Seoul, South Korea

[21] Department of Physics, University of Oslo, Oslo, Norway

[22] Dipartimento di Fisica dell'Università 'La Sapienza' and Sezione INFN Rome, Italy

[23] Dipartimento di Fisica dell'Università and Sezione INFN, Cagliari, Italy

[24] Dipartimento di Fisica dell'Università and Sezione INFN, Trieste, Italy

[25] Dipartimento di Fisica dell'Università and Sezione INFN, Turin, Italy

[26] Dipartimento di Fisica e Astronomia dell'Università and Sezione INFN, Bologna, Italy

[27] Dipartimento di Fisica e Astronomia dell'Università and Sezione INFN, Catania, Italy

[28] Dipartimento di Fisica e Astronomia dell'Università and Sezione INFN, Padova, Italy

[29] Dipartimento di Fisica 'E.R. Caianiello' dell'Università and Gruppo Collegato INFN, Salerno, Italy

[30] Dipartimento di Scienze e Innovazione Tecnologica dell'Università del Piemonte Orientale and Gruppo Collegato INFN, Alessandria, Italy

[31] Dipartimento Interateneo di Fisica 'M. Merlin' and Sezione INFN, Bari, Italy

[32] Division of Experimental High Energy Physics, University of Lund, Lund, Sweden

[33] Eberhard Karls Universität Tübingen, Tübingen, Germany

[34] European Organization for Nuclear Research (CERN), Geneva, Switzerland

[35] Faculty of Engineering, Bergen University College, Bergen, Norway

[36] Faculty of Mathematics, Physics and Informatics, Comenius University, Bratislava, Slovakia

[37] Faculty of Nuclear Sciences and Physical Engineering, Czech Technical University in Prague, Prague, Czech Republic

[38] Faculty of Science, P.J. Šafárik University, Košice, Slovakia

[39] Frankfurt Institute for Advanced Studies, Johann Wolfgang Goethe-Universität Frankfurt, Frankfurt, Germany

[40] Gangneung-Wonju National University, Gangneung, South Korea

[41] Gauhati University, Department of Physics, Guwahati, India

[42] Helsinki Institute of Physics (HIP), Helsinki, Finland

[43] Hiroshima University, Hiroshima, Japan

[44] Indian Institute of Technology Bombay (IIT), Mumbai, India

[45] Indian Institute of Technology Indore, Indore (IITI), India

[46] Institut de Physique Nucléaire d'Orsay (IPNO), Université Paris-Sud, CNRS-IN2P3, Orsay, France

[47] Institut für Informatik, Johann Wolfgang Goethe-Universität Frankfurt, Frankfurt, Germany

[48] Institut für Kernphysik, Johann Wolfgang Goethe-Universität Frankfurt, Frankfurt, Germany

[49] Institut für Kernphysik, Westfälische Wilhelms-Universität Münster, Münster, Germany

[50] Institut Pluridisciplinaire Hubert Curien (IPHC), Université de Strasbourg, CNRS-IN2P3, Strasbourg, France

[51] Institute for Nuclear Research, Academy of Sciences, Moscow, Russia

[52] Institute for Subatomic Physics of Utrecht University, Utrecht, Netherlands

[53] Institute for Theoretical and Experimental Physics, Moscow, Russia

[54] Institute of Experimental Physics, Slovak Academy of Sciences, Košice, Slovakia

[55] Institute of Physics, Academy of Sciences of the Czech Republic, Prague, Czech Republic

[56] Institute of Physics, Bhubaneswar, India

[57] Institute of Space Science (ISS), Bucharest, Romania

[58] Instituto de Ciencias Nucleares, Universidad Nacional Autónoma de México, Mexico City, Mexico

[59] Instituto de Física, Universidad Nacional Autónoma de México, Mexico City, Mexico

[60] iThemba LABS, National Research Foundation, Somerset West, South Africa

[61] Joint Institute for Nuclear Research (JINR), Dubna, Russia

[62] Korea Institute of Science and Technology Information, Daejeon, South Korea

[63] KTO Karatay University, Konya, Turkey
[64] Laboratoire de Physique Corpusculaire (LPC), Clermont Université, Université Blaise Pascal, CNRS–IN2P3, Clermont-Ferrand, France
[65] Laboratoire de Physique Subatomique et de Cosmologie, Université Grenoble-Alpes, CNRS-IN2P3, Grenoble, France
[66] Laboratori Nazionali di Frascati, INFN, Frascati, Italy
[67] Laboratori Nazionali di Legnaro, INFN, Legnaro, Italy
[68] Lawrence Berkeley National Laboratory, Berkeley, CA, United States
[69] Lawrence Livermore National Laboratory, Livermore, CA, United States
[70] Moscow Engineering Physics Institute, Moscow, Russia
[71] National Centre for Nuclear Studies, Warsaw, Poland
[72] National Institute for Physics and Nuclear Engineering, Bucharest, Romania
[73] National Institute of Science Education and Research, Bhubaneswar, India
[74] Niels Bohr Institute, University of Copenhagen, Copenhagen, Denmark
[75] Nikhef, National Institute for Subatomic Physics, Amsterdam, Netherlands
[76] Nuclear Physics Group, STFC Daresbury Laboratory, Daresbury, United Kingdom
[77] Nuclear Physics Institute, Academy of Sciences of the Czech Republic, Řež u Prahy, Czech Republic
[78] Oak Ridge National Laboratory, Oak Ridge, TN, United States
[79] Petersburg Nuclear Physics Institute, Gatchina, Russia
[80] Physics Department, Creighton University, Omaha, NE, United States
[81] Physics Department, Panjab University, Chandigarh, India
[82] Physics Department, University of Athens, Athens, Greece
[83] Physics Department, University of Cape Town, Cape Town, South Africa
[84] Physics Department, University of Jammu, Jammu, India
[85] Physics Department, University of Rajasthan, Jaipur, India
[86] Physik Department, Technische Universität München, Munich, Germany
[87] Physikalisches Institut, Ruprecht-Karls-Universität Heidelberg, Heidelberg, Germany
[88] Politecnico di Torino, Turin, Italy
[89] Purdue University, West Lafayette, IN, United States
[90] Pusan National University, Pusan, South Korea
[91] Research Division and ExtreMe Matter Institute EMMI, GSI Helmholtzzentrum für Schwerionenforschung, Darmstadt, Germany
[92] Rudjer Bošković Institute, Zagreb, Croatia
[93] Russian Federal Nuclear Center (VNIIEF), Sarov, Russia
[94] Russian Research Centre Kurchatov Institute, Moscow, Russia
[95] Saha Institute of Nuclear Physics, Kolkata, India
[96] School of Physics and Astronomy, University of Birmingham, Birmingham, United Kingdom
[97] Sección Física, Departamento de Ciencias, Pontificia Universidad Católica del Perú, Lima, Peru
[98] Sezione INFN, Bari, Italy
[99] Sezione INFN, Bologna, Italy
[100] Sezione INFN, Cagliari, Italy
[101] Sezione INFN, Catania, Italy
[102] Sezione INFN, Padova, Italy
[103] Sezione INFN, Rome, Italy
[104] Sezione INFN, Trieste, Italy
[105] Sezione INFN, Turin, Italy
[106] SSC IHEP of NRC Kurchatov institute, Protvino, Russia
[107] SUBATECH, Ecole des Mines de Nantes, Université de Nantes, CNRS-IN2P3, Nantes, France
[108] Suranaree University of Technology, Nakhon Ratchasima, Thailand
[109] Technical University of Split FESB, Split, Croatia
[110] The Henryk Niewodniczanski Institute of Nuclear Physics, Polish Academy of Sciences, Cracow, Poland
[111] The University of Texas at Austin, Physics Department, Austin, TX, USA
[112] Universidad Autónoma de Sinaloa, Culiacán, Mexico
[113] Universidade de São Paulo (USP), São Paulo, Brazil
[114] Universidade Estadual de Campinas (UNICAMP), Campinas, Brazil
[115] University of Houston, Houston, TX, United States

[116] University of Jyväskylä, Jyväskylä, Finland
[117] University of Liverpool, Liverpool, United Kingdom
[118] University of Tennessee, Knoxville, TN, United States
[119] University of Tokyo, Tokyo, Japan
[120] University of Tsukuba, Tsukuba, Japan
[121] University of Zagreb, Zagreb, Croatia
[122] Université de Lyon, Université Lyon 1, CNRS/IN2P3, IPN-Lyon, Villeurbanne, France
[123] V. Fock Institute for Physics, St. Petersburg State University, St. Petersburg, Russia
[124] Variable Energy Cyclotron Centre, Kolkata, India
[125] Vestfold University College, Tonsberg, Norway
[126] Warsaw University of Technology, Warsaw, Poland
[127] Wayne State University, Detroit, MI, United States
[128] Wigner Research Centre for Physics, Hungarian Academy of Sciences, Budapest, Hungary
[129] Yale University, New Haven, CT, United States
[130] Yonsei University, Seoul, South Korea
[131] Zentrum für Technologietransfer und Telekommunikation (ZTT), Fachhochschule Worms, Worms, Germany